Mechanical Properties and Morphology of PA6/EVA Blends

ARUP R. BHATTACHARYYA,[1] S. N. MAITI,[1] ASHOK MISRA[2]

[1] Centre for Polymer Science and Engineering, Indian Institute of Technology Delhi, New Delhi, India, 110016

[2] Indian Institute of Technology Bombay, India, 400076

Received 26 February 2001; accepted 29 October 2001

ABSTRACT: The mechanical properties of blends of polyamide6 (PA6) and ethylene vinyl acetate (EVA) at a blending composition of 0–50 wt % EVA were studied. The notched Izod impact strength of PA6 increased with the incorporation of EVA, the increase being more than 100% compared to PA6 at 10% EVA. The tensile strength and the tensile modulus of the blends decreased steadily as the weight percent of EVA increased. Analysis of the tensile data using predictive theories indicated the extent of the interaction of the dispersed phase and the matrix up to 20 wt % EVA. SEM studies of the cryogenically fractured surfaces indicated increase in the dispersed phase domain size with EVA concentrations. On the other hand, impact fractured surfaces of PA6/EVA blends indicated debonding of EVA particles, leaving hemispherical bumps, indicating inadequate interfacial adhesion between PA6 and EVA. © 2002 Wiley Periodicals, Inc. J Appl Polym Sci 85: 1593–1606, 2002

Key words: polyamide 6/ethylene vinyl acetate blends; impact toughening; mechanical properties; phase morphology

INTRODUCTION

Polyamide6 (PA6) is a versatile engineering plastic with a wide range of useful properties.[1] However, the most glaring limitation of the polymer is its low impact strength below the glass transition temperature.[2] Melt blending with a large variety of rubbery polymers is widely used to improve the impact strength of PA6, particularly at low temperatures.[2–4] It is reported that the tensile strength and tensile modulus decrease approximately proportionally to the rubber concentration in the rubber-toughened PA6 systems.[5,6] The impact strength of PA6/rubber blends depends on the rubber concentration, rubber particle size, particle-size distribution, and the adhesion between the two phases.[4] It was shown that PA6 could be toughened with a dispersed rubber having a particle size of 0.1–2 μm.[7] The effect of the concentration and the particle size of the rubber on the brittle–tough transition temperature of PA6/ethylene propylene diene copolymer (EPDM) blends was investigated by Borggreve et al.[8] The brittle–tough transition temperature shifted to lower values when the rubber content was increased or the rubber particle size decreased. A correlation was found between the brittle–tough transition temperature and the interparticle distance. The deformation mechanism during fracture in PA6/rubber blends was investigated by several workers.[9–11] The molecular architecture and morphological aspects on the plastic deformation mechanism of rubber-toughened thermoplastic polymers were reviewed by Groeninckx and Dompas.[12] In a correlation study between the mechanical properties of the elastomer and the impact behavior of the elastomer-modified PA6, the type of the impact modifier influenced the impact

Correspondence to: A. Misra (amisra@cc.iitb.ac.in).

Journal of Applied Polymer Science, Vol. 85, 1593–1606 (2002)

behavior of the blend.[13] The effect of the rubber type and morphology on the impact property of PA6-based blends was investigated by several authors.[14–16]

In the present article, the effects of the ethylene vinyl acetate (EVA) copolymer on the mechanical and morphological properties of PA6/EVA blends are reported. Mechanical properties such as impact strength, tensile behavior, and flexural properties were studied as a function of EVA concentrations. Morphological analysis of the blends was carried out by scanning electron microscopic (SEM) studies.

EXPERIMENTAL

Materials

Polyamide6 (PA6) was obtained from M/s Gujarat State Fertilizer Corp. (Baroda, India; GUJLON M28RC, relative viscosity 2.8). EVA with a vinyl acetate (VA) content of 18 wt % and an MFI of 2 g/10 min (EVA 1802) from M/s National Organic Chemical Industries Ltd. (Mumbai, India) was used as the blending polymer. The polymers were dried in a vacuum oven at 80^0C for over 24 h.

Blending

The granules were dry-mixed in appropriate ratios, and blends of PA6 and EVA were prepared using a corotating, intermeshing twin-screw extruder (ZSK25, L/D = 46) at 230^0C and a screw speed of 150 rpm. The time for blending was approximately 2 min. The EVA level was varied from 0 to 50 wt % (0–0.548 vol %) in the binary blends of PA6/EVA. The extruded strands were quenched immediately after extrusion in a water bath kept at room temperature. The extrudates were then chopped into granules and finally dried at 80^0C for over 24 h before molding. Individual polymers were also extruded under identical conditions to ensure the same thermal history as that of the blend compositions.

Preparation of Test Specimens

Test specimens used for mechanical properties investigation were prepared by injection molding at 230^0C and at a screw speed of 80 rpm with a cooling time of 60 s.

Measurements

Tensile properties were measured on an Instron Universal Tester (Model 4301) according to the ASTM D-638, type 1, procedure at an extension rate of 50 mm/min. Notched izod impact strength was measured on a CEAST impact tester (Model Resil 25) following ASTM D-256 test procedures. All impact strength measurements were made at five different temperatures (−25, 0, 23, 40, and 80^0C). Each of the samples was kept in a vacuum oven at each test temperature for 4 h prior to impact testing. The test results reported are the average values of at least five specimens tested in each case to obtain a reliable value. The deviation of the data around the mean value was less than 5%. Morphological studies were conducted by SEM using a Cambridge Stereoscan microscope (Model S4-10). For morphological analysis, cryogenically fractured tensile specimens etched by *o*-xylene to remove EVA and impact-fractured specimens were used. For each blend, different micrographs with a total amount of around 200 particles were made. These micrographs were analyzed using a camera attached with image analysis software and the diameter of the particles was determined. Number-average diameter (D_n) and weight-average diameter (D_w) of the domain were determined according to the following relationships:

$$D_n = \sum N_i D_i / \sum N_i \tag{1}$$

$$D_w = \sum N_i D_i^2 / \sum N_i D_i \tag{2}$$

The interfacial area (A_{3D}) per unit volume of the dispersed phase (V_{3D}) was calculated from the total perimeter of the particles (P_{2D}) divided by the total area of the particles (A_{2D}) as obtained from the micrographs:

$$A_i(\mu m^2/\mu m^3) = P_{2D}/A_{2D} = A_{3D}/V_{3D} \tag{3}$$

The critical interparticle distance (IPDC) was calculated from Wu's equation:[7]

$$\text{IPDC} = d[(3.14/6\varphi_r)^{1/3} - 1] \tag{4}$$

where d is the average diameter of the domain and ϕ_r is the volume fraction of the dispersed phase.

RESULTS AND DISCUSSION

Impact Properties

The plots of the notched Izod impact strength for PA6/EVA binary blends as functions of weight

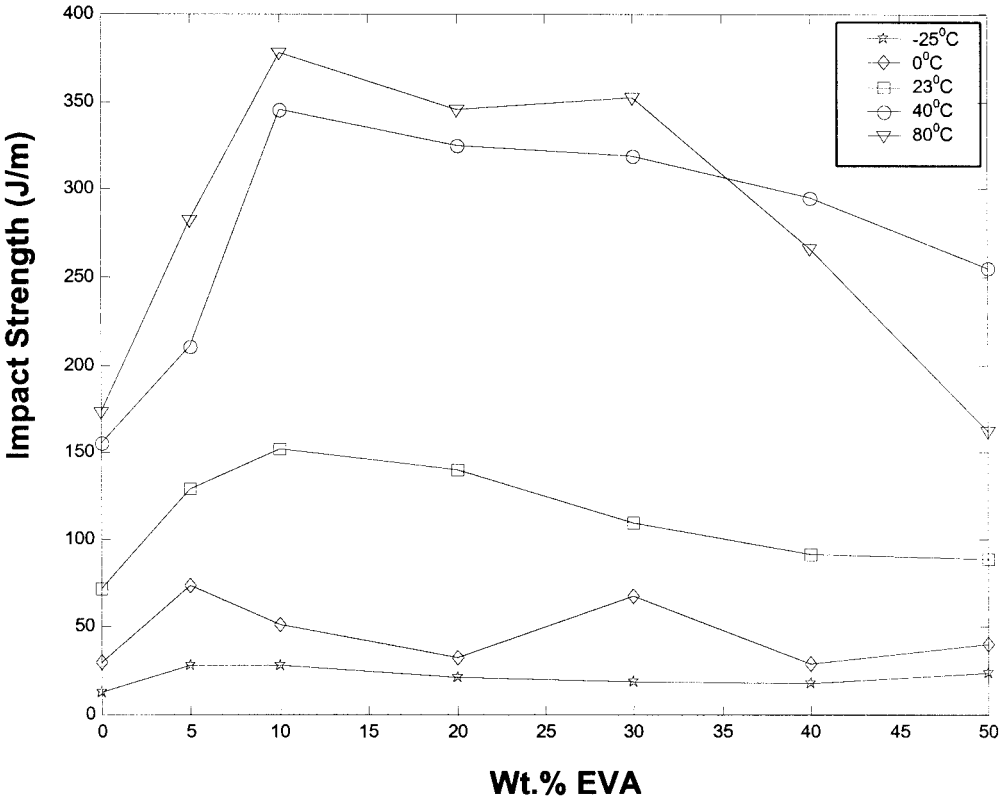

Figure 1 Plot of notched impact strength versus blend compositions at different temperatures.

percent EVA and temperature are presented in Figures 1 and 2, respectively. All the blend compositions together with pure PA6 exhibited the lowest value at -25^0C. The impact strength values increased with increasing temperature (Fig. 1). On addition of EVA, the notched impact strength of the blends increased at all levels. The increase in impact strength at 23^0C was maximum for a 90/10 combination of PA6/EVA, the value being about twice higher than that of pure PA6. The variation in the notched impact strength of the blends with the EVA level was generally similar at all the test temperatures. On increasing the test temperature, all the compositions showed higher values as compared to the values obtained at lower temperature. At 23^0C, the notched impact strength of PA6 increased at all levels of EVA, the value being 1.2–2.1 times that of pure PA6 depending on the blend composition. As seen in Figure 2, the brittle-to-tough transition temperature (T_{bt}) values of all the blend compositions were around 40^0C, which is very near the T_g of PA6: 48^0C. At this temperature, PA6 also exhibited the highest impact strength, in agreement with the reported literature that most crystalline polymers show greater impact strength in the neighborhood of the T_g. This is attributed to the fact that at temperatures around or above the T_g the molecular motions are significantly high to relieve stress concentrations.[8] At this temperature, the notched Izod impact strength of these blends increased significantly, indicating tough behavior. It has been reported that for a series of PA6/EPDM blends the observed impact behavior at 23^0C was poor since the brittle-to-tough transition temperature was around 45^0C.[8] This behavior was explained on the basis of a relatively large particle size, or due to low interfacial adhesion, or the combined effect of both of the parameters, as has been shown in morphological analysis. In PA6/EVA blends, the interfacial adhesion between the two phases is believed to be the predominant factor in enhancing the impact strength. It is also reported that the brittle-to-tough transition temperature is no longer induced by rubber particles if the temperature approaches the T_g value of PA6 and a critical interparticle distance has little significance.[8]

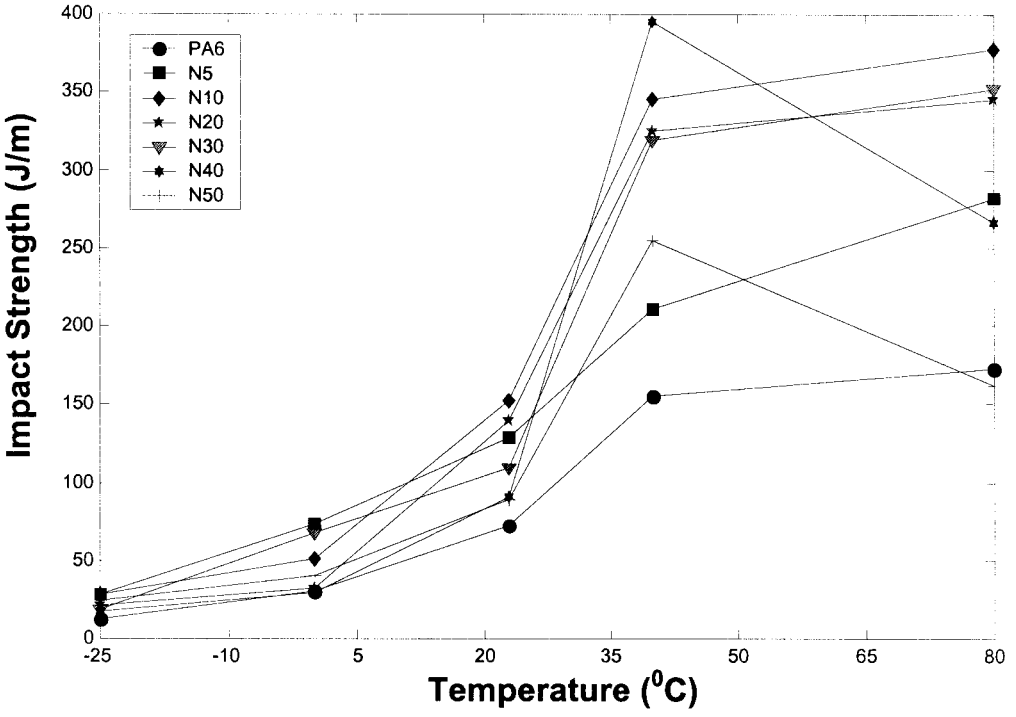

Figure 2 Plot of notched impact strength versus temperature at 0–50 wt % EVA level.

In the PA6/EVA blends, increase in the notched impact strength can be attributed to EVA particles acting as stress concentrators, thus exploiting the rubbery nature of EVA. The deformation process in pure PA6 is by shear yielding. In PA6/EVA blends, during impact, the deformation is triggered (initiated) by yielding of the PA6 matrix where the EVA phase also participated via an energy-absorption process caused by the EVA particles.

Tensile Properties

Tensile stress–strain curves are shown in Figure 3. Various tensile properties such as stress at peak, stress at break, tensile modulus, and elongation at break determined from these curves are presented in Table I. It is observed from Figure 3 that both pure PA6 and EVA show ductile failure in tension. PA6 exhibits a prominent yield point, whereas, in the case of EVA, the stress–strain curve is typical of that of a rubbery polymer, having no yield point with 400% elongation at break. On incorporation of EVA up to 20 wt %, the binary blends showed lower yield stress with broadening of the yield peak, accompanied by higher elongation at break as compared to pure PA6. Beyond 20 wt % EVA, the blends exhibited even lower yield stress with decreased rubbery deformation, but the mode of failure remained ductile. It was found from the stress–strain curves that the work of rupture of PA6 increased on incorporation of EVA to 20 wt % in the PA6/EVA binary blends. The higher values of toughness in the blends may be correlated with the increased value of elongation at break of the blends up to a 20 wt % EVA level.

It can be seen from Table I and Figures 4 and 5 that the stress at peak, stress at break, and tensile modulus of the binary blends decrease with incorporation of EVA. The decrease of tensile strength [stress at peak, Fig. 4(a)] is negligible at the 5 wt % EVA level and the decrease in tensile strength is 22–64% as the EVA content increases from 20 to 50 wt %, depending on the blend composition. In a similar way, the decrease in tensile modulus (Fig. 5) is 30–64% as the EVA content varies from 20 to 50 wt %. The lowering of the tensile strength in the PA6/EVA blends may be attributed to the presence of rubbery EVA particles acting as stress concentrators, which result in yielding at an overall stress lower than that for pure PA6. The decrease in the tensile modulus in

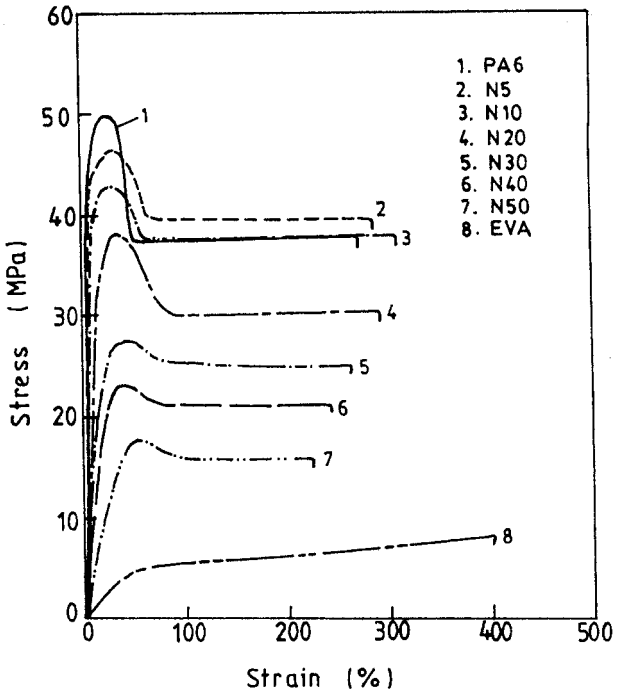

Figure 3 Stress–strain curves of PA6/EVA blends.

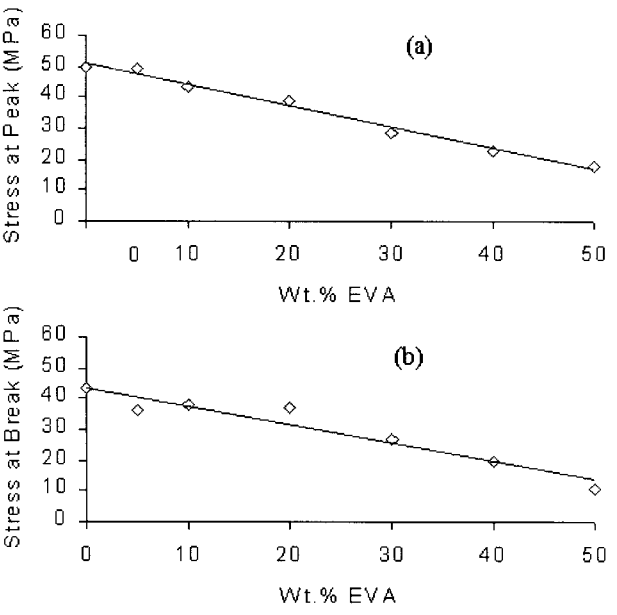

Figure 4 (a) Plot of stress at peak versus weight percent EVA; (b) plot of stress at break versus weight percent EVA.

the blends may be accounted for by the softening effect of the EVA copolymer, since the tensile modulus of EVA is considerably lower than that of pure PA6. The introduction of EVA, a low modulus material, in the PA6 matrix causes an overall lowering in the tensile modulus of the blends. The low interfacial adhesion between the two mixtures also contributes to this.

Theoretical Analysis of Tensile Strength (Stress at Peak)

Predictive models were used to analyze the tensile strength data of polymer blends to assess the level of interfacial interaction. Kunori and Geil[17] used such models to analyze blends of polycarbonate and high-density polyethylene as well as the blends of polycarbonate and polystyrene. Other reported studies also used similar models in polymer blends and composites.[18–20] Three models used to analyze the tensile strength results obtained in this study are as follows:

Model 1: Neilsen's first power-law model[21]:

$$\frac{\sigma_b}{\sigma_p} = (1 - \phi_1)S \tag{5}$$

Model 2: Neilsen's two-third power-law model[21]:

Table I Mechanical Properties of PA6/EVA Blends

Sample Code	Composition PA6/EVA (wt %)	Stress at Peak (MPa)	Stress at Break (MPa)	Strain at Break (%)	Tensile Modulus (MPa)	Flexural Strength (MPa)	Flexural Modulus (MPa)
N100	100/0	50	43	273	1176	42	1092
N5	95/5	49	36	282	1103	34	920
N10	90/10	43	38	305	975	29	895
N20	80/20	39	37	290	820	26	790
N30	70/30	29	27	255	636	22	685
N40	60/40	23	20	245	521	22	685
N50	50/50	18	11	225	422	16	584

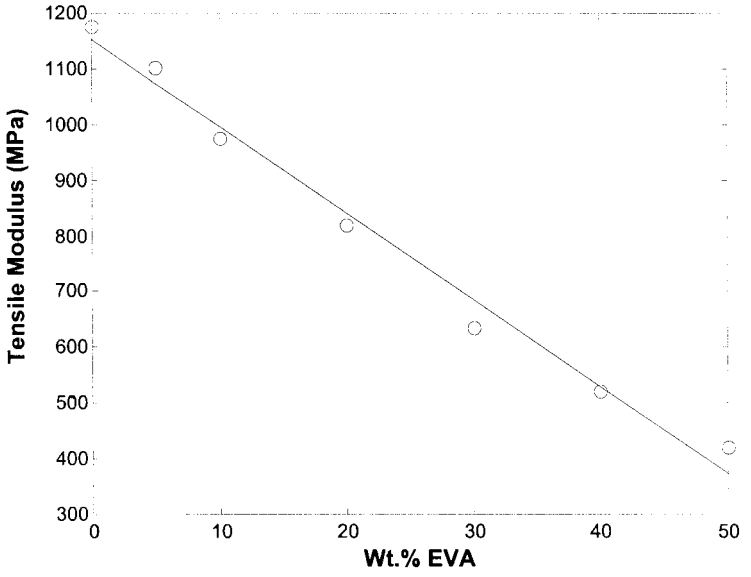

Figure 5 Plot of tensile modulus versus weight percent EVA.

$$\frac{\sigma_b}{\sigma_p} = (1 - \phi^{2/3}{}_1)S' \tag{6}$$

Model 3: Nicolais and Narkis model[22]:

$$\frac{\sigma_b}{\sigma_p} = (1 - K_b\phi_1^{2/3}) \tag{7}$$

where σ_b and σ_p represent the tensile strength of the blend and PA6, respectively, and ϕ_1, the volume fraction of EVA in the blends. S and S' are the Neilsen parameters in the first and two third power-law models, respectively, which account for the weakness in the structure brought about by the discontinuity in stress transfer and generation of stress concentration at the interfaces in case of composites and blends. The maximum value of S and S' is unity for no stress concentration effect. K_b in eq. (7) is an adhesion parameter; the maximum value of K_b is 1.21 for spherical inclusion of the minor phase having no adhesion.[22] The three models described above were employed to analyze the tensile strength results in order to evaluate interfacial adhesion, if any, by comparing the experimental values with those predicted by the models. The values of S, S', and K_b are listed in Table II, giving a comparison between the experimental data and theoretical models. Plots of relative tensile strength (σ_b/σ_p) versus ϕ_1 of the blends predicted using these models are presented in Figures 6–8.

In Figure 6, σ_b/σ_p values predicted from model 1 with $S = 1$, $S = 0.94$, and experimental results are plotted as a function of ϕ_1. The line with $S = 1$

Table II Values of Stress-concentration Parameters (S, S', and K_b) in PA6/EVA Blends

Sample Code	Wt % EVA	Volume Fraction of EVA (Φ)	S	S'	K_b
N100	0	0	0	0	0
N5	5	0.06	1.04	1.15	0.137
N10	10	0.119	0.97	1.13	0.586
N20	20	0.233	1.01	1.25	0.589
N30	30	0.342	0.92	1.19	0.797
N40	40	0.456	0.85	1.14	0.902
N50	50	0.548	0.84	1.12	0.938
Mean	—	—	0.94	1.16	0.66

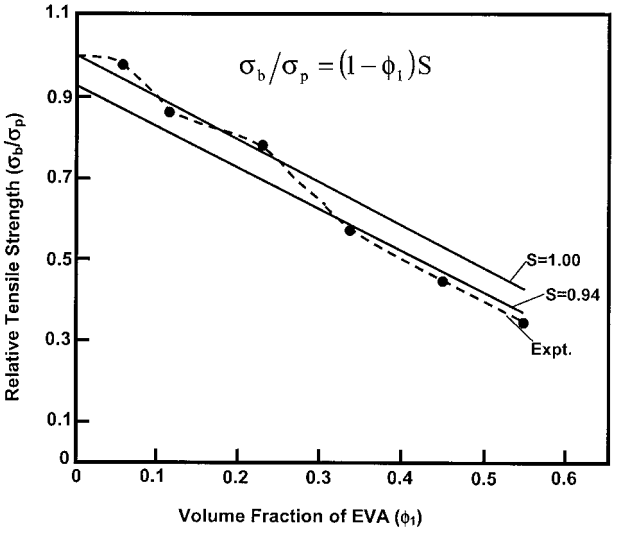

Figure 6 Plot of relative tensile strength versus volume fraction of EVA using Model 1.

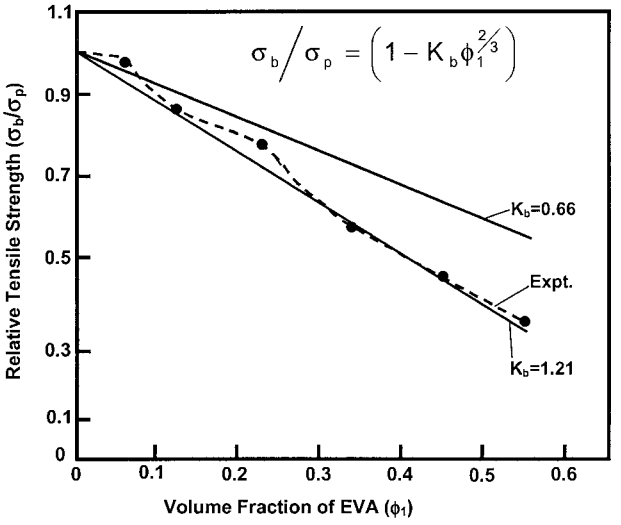

Figure 8 Plot of relative tensile strength versus volume fraction of EVA using Model 3.

represents perfect adhesion. The experimental values are slightly higher than those predicted from the above equations with $S = 1$ and 0.94 up to $\phi_1 = 0.23$, being closer to the line $S = 1$. For higher EVA content, the σ_b/σ_p values are lower than the predicted curves, but closer to the line $S = 0.94$. The experimental data exhibit a reasonably good fit with the predictive model with $S = 1$ up to $\phi_1 = 0.23$, whereas for $\phi_1 > 0.3$, the data deviate and lie around the curve with $S = 0.94$. It seems, therefore, that the blend is converted from a no-stress concentration system to a structure with significant stress concentration around the EVA level of 0.23–0.3. This shows that at an EVA content higher than 0.23 the blends cannot take excessive stress since the interfacial adhesion is lowered.

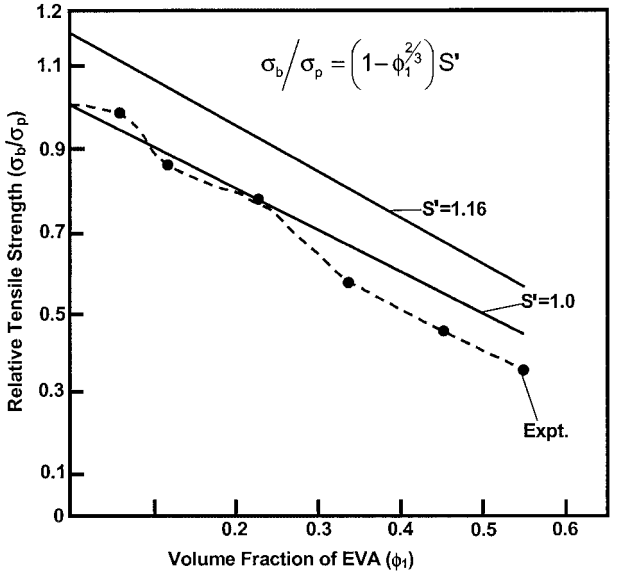

Figure 7 Plot of relative tensile strength versus volume fraction of EVA using Model 2.

In Figure 7, the relative tensile strength values predicted from Model 2 with $S' = 1$, $S' = 1.16$, and experimental results are plotted versus ϕ_1. The experimental data were around the line with $S' = 1$ up to $\phi_1 = 0.23$, but the values decrease at $\phi_1 > 0.3$. The experimental data are considerably below the line with $S' = 1.16$. This is again in favor of adequate interfacial adhesion in the blends up to an EVA level of 0.23. Thus, by comparing the values of Neilsen's parameters (S & S') of the two power laws, it is found that the extent of deviation of the S value from 1 is less than that of the S' value, which implies that the first power-law model is more suitable than is the fractional power-law model in describing the tensile stress data.

The third model has a weightage factor K_b that represents the dispersed phase as spherical inclusions. When there is no adhesion of the inclusions to the matrix, $K_b = 1.21$. The analysis shows an average value of K_b to be 0.66, which is much less than 1.21. This implies an extent of enhanced interaction between the phases up to $\phi_1 = 0.23$. In Figure 8, the relative tensile strength values predicted from model 3 with $K_b = 1.21$, $K_b = 0.66$, and the experimental results are plotted as a

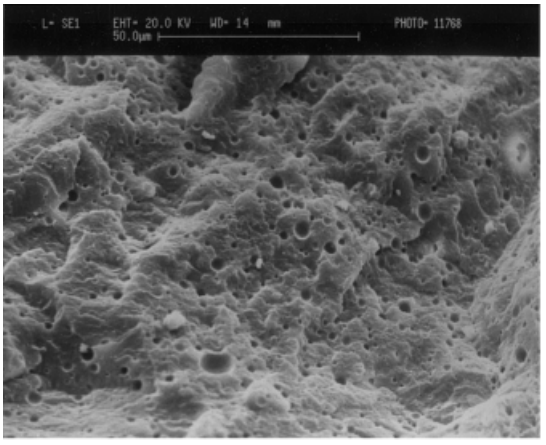

(a) PA6/EVA (95/5)

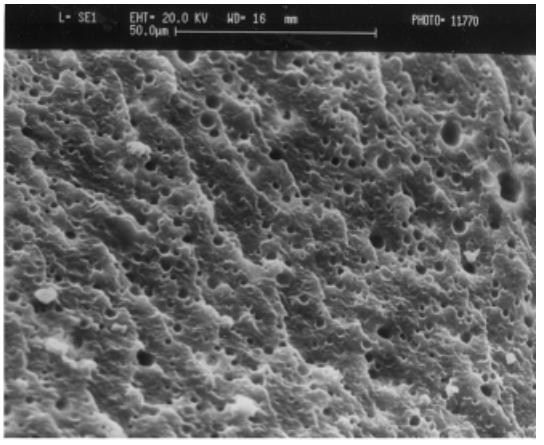

(b) PA6/EVA (90/10)

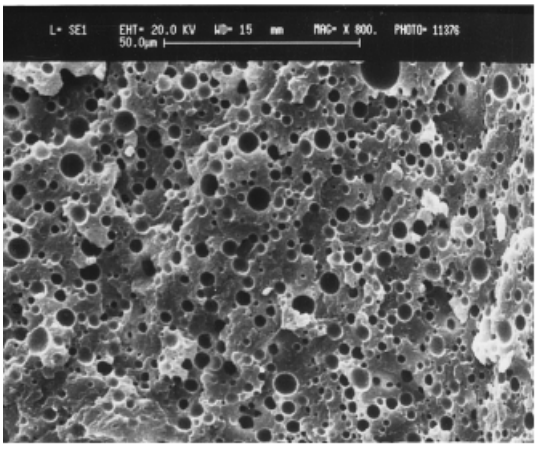

(c) PA6/EVA (80/20)

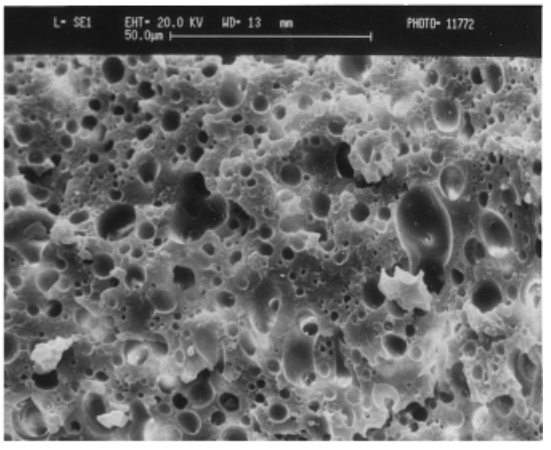

(d) PA6/EVA (70/30)

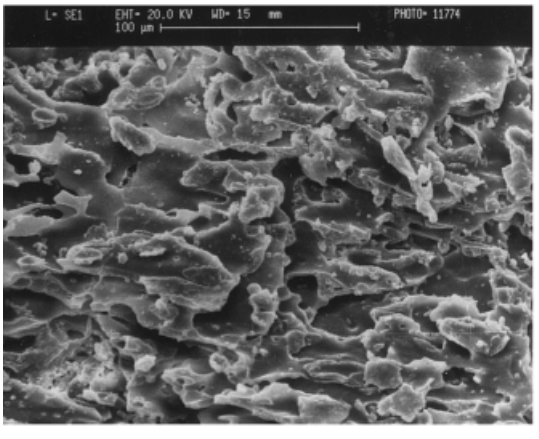

(e) PA6/EVA (60/40)

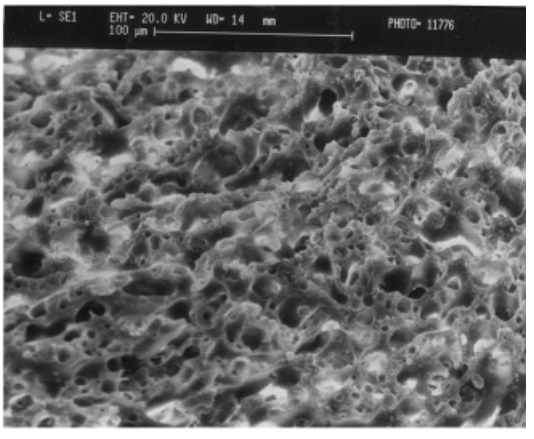

(f) PA6/EVA (50/50)

Figure 9 SEM photomicrographs of cryogenically fractured etched surfaces of PA6/EVA blends.

Table III Morphological Parameters from SEM Analysis

Sample Code	Composition, PA6/EVA, (wt %)	D_n (μm)	D_w (μm)	D_w/D_n	A_i ($\mu m^2/\mu m^3$)	IPDC (μm)
N5	95/5	1.24	1.73	1.39	0.14	1.29
N10	90/10	1.43	2.05	1.43	0.24	0.90
N20	80/20	1.80	2.70	1.50	0.38	0.55
N30	70/30	2.70	7.28	2.69	0.38	0.40

function of ϕ_1. Beyond $\phi_1 = 0.23$, the data deviate from the model with $K_b = 0.66$ and lie closer to the line with $K_b = 1.21$. This indicates the reduction of interphase interaction, probably due to the coalescence and sequential larger domain formation of the EVA phase (shown later).

Flexural Properties

The flexural strength and modulus of PA6 decreased on incorporation of EVA in the PA6/EVA binary blends, as presented in Table I. The trend is along similar lines as that of the decrease of the tensile strength and modulus in the binary blends. The decrease of the flexural modulus and strength is about 29–60% and 50–66%, respectively, as the EVA content varies from 20 to 50 wt %. Deterioration of the flexural properties may be attributed to the incorporation of the rubbery EVA phase to the hard-plastic phase PA6, increasing the deformability of the latter.

Phase Morphology

This section deals with the morphological studies carried out on the PA6/EVA binary blend systems with the EVA level varying from 0 to 50 wt %. The scanning electron micrographs of the cryogenically fractured etched surfaces of PA6/EVA blends are presented in Figure 9. The SEM analysis of cryogenically fractured etched surfaces show two different types of morphology in these blends. A particle-dispersed morphology was observed in blends with EVA levels from 5 to 30 wt %, as seen in Figure 9(a–d). On the other hand, a cocontinuous morphology was observed at an EVA level of 40–50 wt % [Fig. 9(e,f)]. The morphological parameters obtained from SEM analysis of cryogenically fractured etched surfaces are presented in Table III. The EVA domain size distribution in the blends of PA6/EVA at different levels of EVA was determined and is presented in Figure 10. The variations of the average domain size and interfacial area with varying levels of EVA are presented in Figures 11 and 12, respectively.

The parameters D_n, D_w, A_i, and IPDC are given in Table III. The D_n of EVA increased in the PA6 matrix with the EVA level. The value of D_n increased from 1.24 μm at 5 wt % EVA to 2.70 μm at 30 wt % of EVA. It is also evident from Figure 10 that the domain size distribution of the EVA phase increases monotonically at a higher EVA content in the PA6/EVA blends, probably due to coalescence of the EVA particles and high interfacial tension between PA6 and EVA. Furthermore, Figure 11 shows an increase in D_w with the EVA concentration, being highest for the 70/30 PA6/EVA blend, which is much higher than is the corresponding D_n. This indicates a wider domain size distribution at this composition, probably due to a greater degree of coalescence, similar to those reported for other blends.[23,24]

The parameter A_i increased marginally with the incorporation of EVA to 20 wt %, as seen in Figure 12. It is reported that A_i is a measure of the interfacial thickness in the multiphase polymer systems.[25] PA6/EVA blends form a narrow interface due to the incompatibility between the components, which is reflected in the lower values of A_i (Table III).

According to Wu's theory, the brittle-to-tough transition temperature of the blends depends on the critical matrix ligament thickness (IPDC). If the matrix ligament thickness value is lower than is the critical value, the blends would be tough, while if it is above the critical value, the blend would be brittle. It has also been reported that the critical value of the ligament thickness of PA66/rubber blends is about 0.3 μm.[7] It is observed from Table III that the IPDC for the PA6/EVA blends is higher than 0.3 μm. To make the blends tough, the ligament thickness should be reduced to below 0.3 μm. Thus, the blends of PA6/EVA would show brittle behavior. It may also be noted that if the interfacial adhesion between the two phases is low enough then the critical ligament

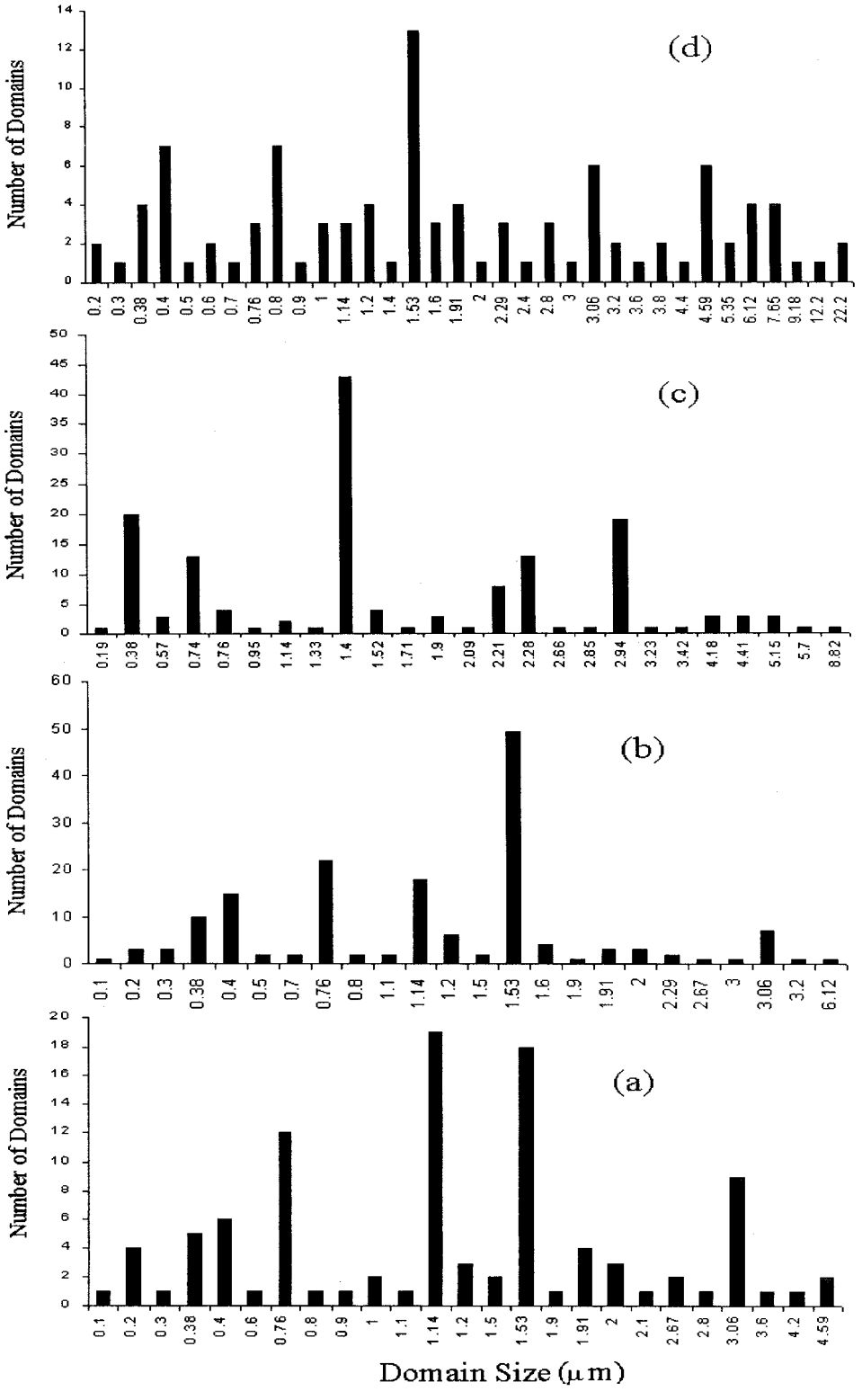

Figure 10 Average domain size distribution of PA6/EVA blends: (a) 95/5; (b) 90/10; (c) 80/20; (d) 70/30.

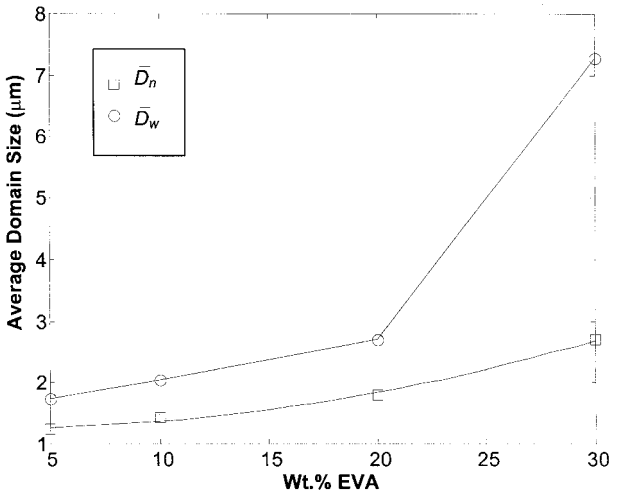

Figure 11 Plot of average domain size versus weight percent EVA.

thickness parameter value may not explain the brittle/tough behavior in the PA6/rubber blends. The occurrence of cocontinuous morphology at the EVA level of 30–50 wt % is believed to be due to a higher rate of coalescence with increase in the EVA level. The morphological parameters of the blends of an EVA level higher than 30 wt % could not be calculated due to the cocontinuous nature of the blends.

Fracture Surface Analysis

SEM photomicrographs of notched impact fractured surfaces at 23^0C of the PA6/EVA blends are presented in Figure 13. Pure PA6 exhibits ductile fracture while PA6/EVA blends show debonding of EVA particles with hemispherical bumps, indicating little adhesion between PA6 and EVA. This observation is found up to an EVA level of 30 wt % [Fig. 13(a–e)]. The impact fractured topology of the PA6/EVA blends at an EVA level higher than 30 wt % show a different perspective, indicating rod-shaped particles protruding from the surface or lump of debonded EVA along with some spherical debonded EVA particles. This behavior may be due to the cocontinuous nature of the dispersed phase in these blends. This kind of morphological observation was also seen in PC/HDPE blends, suggesting a brittle, low-energy fracture.[17] It is also evident from the micrographs that the deformation pattern during impact testing in PA6/EVA blends up to a 20 wt % EVA level is of similar type as that of pure PA6. On the other hand, the deformation pattern has changed considerably at EVA levels of more than 20 wt % and is characterized by brittle fracture. There is little sign of plastic deformation or cavitation of the EVA particles.

CONCLUSIONS

The major conclusions of the present study are as follows:

1. In the PA6/EVA blends, the notched Izod impact strength of PA6 increased on the

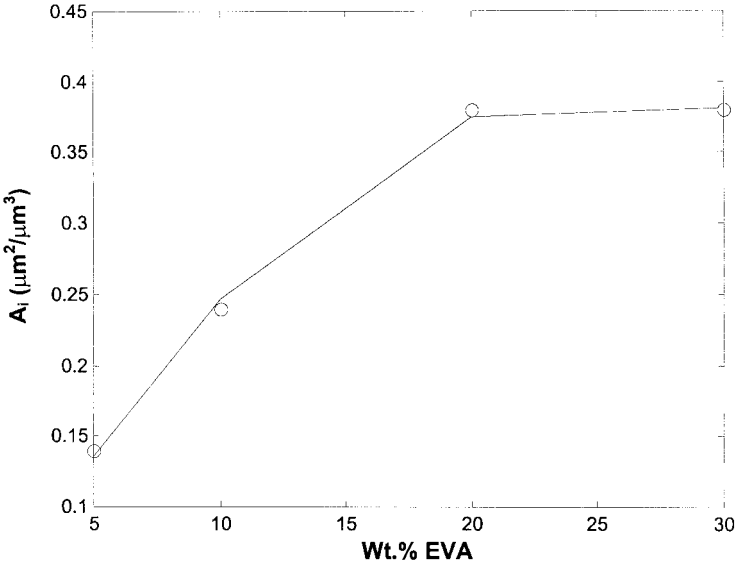

Figure 12 Plot of interfacial area versus weight percent EVA.

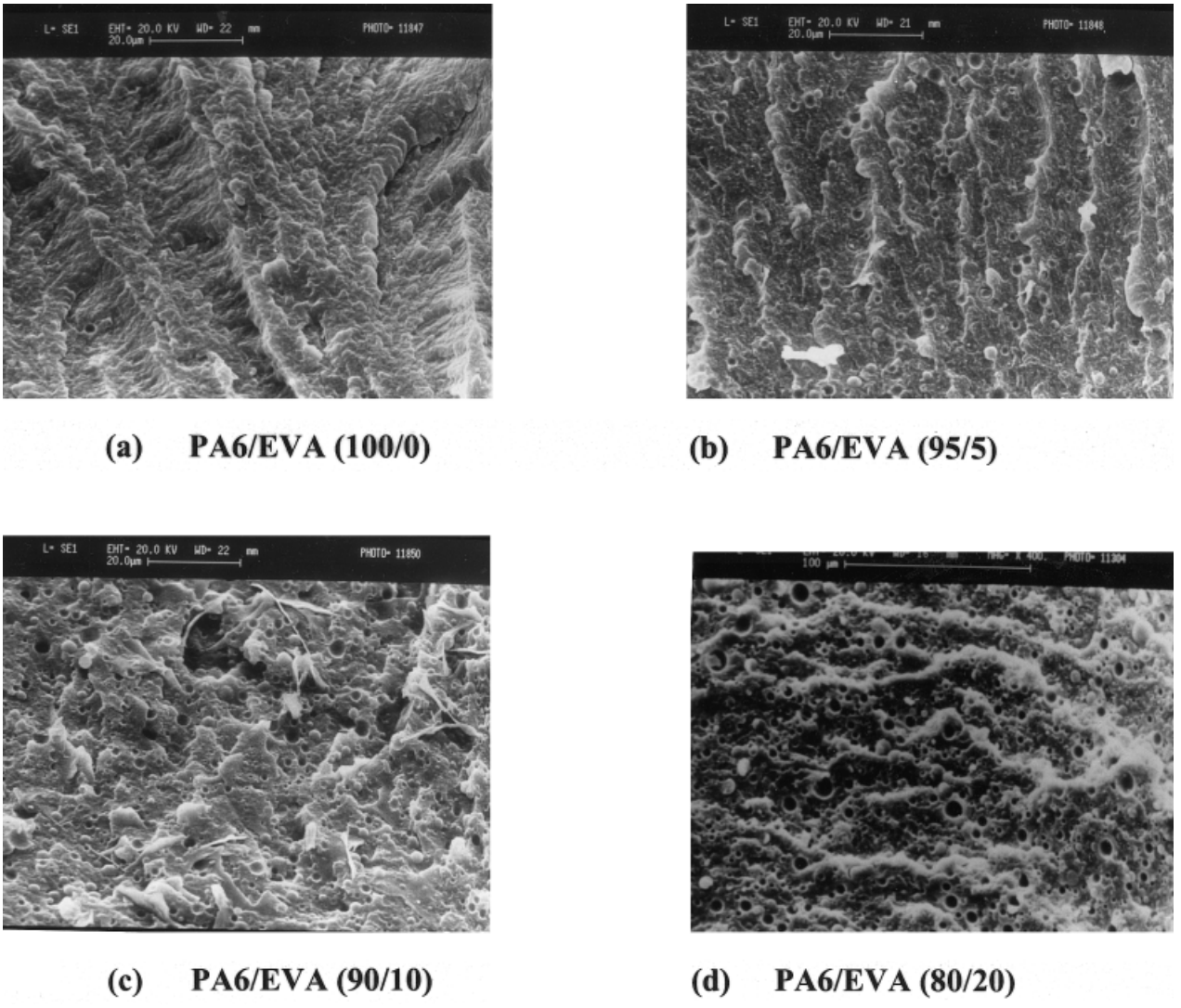

Figure 13 SEM photomicrographs of impact fractured surfaces of PA6/EVA blends.

addition of the EVA copolymer accompanied by a steady decrease of tensile and flexural properties.

2. The maximum impact strength was found at a 90/10 combination of PA6/EVA, being about twice higher than that of pure PA6. The brittle-to-tough transition temperature was about 40^0C for the PA6/EVA blends. The increase in impact strength in PA6 is explained on the basis of better stress transfer in the presence of a rubbery polymer like EVA.
3. The theoretical analysis of tensile properties suggests that there is an extent of interaction between PA6 and EVA up to about a 20 wt % EVA level, whereas the interfacial adhesion decreased at an EVA level of more than 20 wt %.
4. The morphological study as revealed by SEM showed a two-phase morphology, the nature of which is dependent on the composition. In the case of a particle-dispersed morphology, the average domain size of EVA increased with an increasing EVA level. This indicates the pronounced effect of coalescence, which is also evident from a wider domain size distribution at a higher EVA content.

Thus, it may be concluded that the EVA copolymer increased the notched impact strength; however, the extent of impact modification is min-

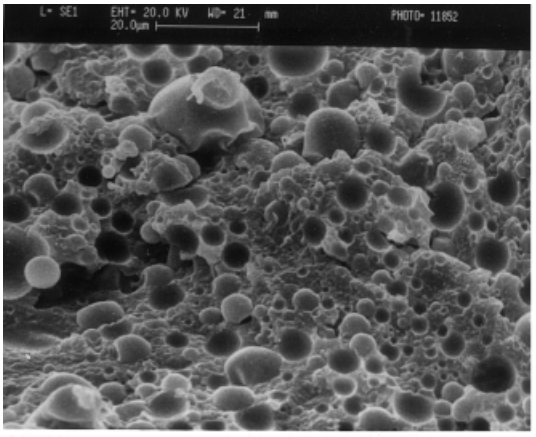

(e) PA6/EVA (70/30)

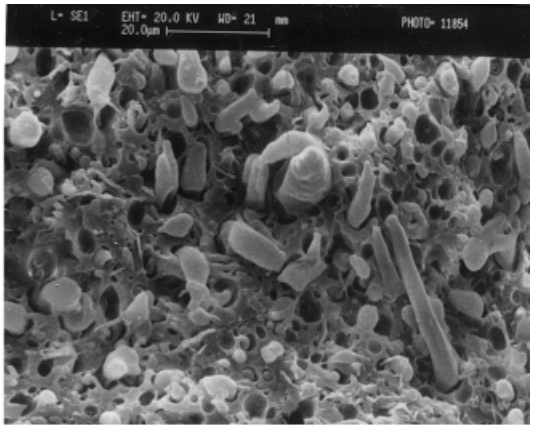

(f) PA6/EVA (60/40)

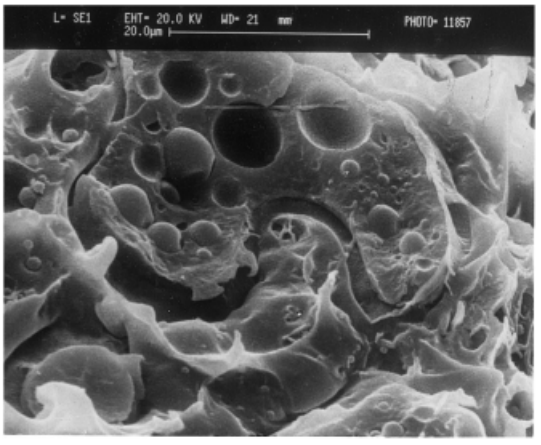

(g) PA6/EVA (50/50)

Figure 13 (*Continued from the previous page*)

imal due to its immiscibility/incompatibility with PA6 accompanied by a reduction of tensile and flexural properties. To obtain higher impact strength, the blends of PA6 and EVA need to be compatibilized, which forms part of a continuation of this study and has been published elsewhere.[26, 27]

REFERENCES

1. Kohan, M. I. Nylon Plastics; SPE Monograph; Wiley: New York, 1973.
2. Paul, D. R.; Newman, S. Polymer Blends; Academic: New York, 1978; Vol. 1.
3. Oshinski, A. J.; Keskkulla, H.; Paul, D. R. Polymer 1996, 37, 4909.
4. Gaymans, R. J. In Rubber Toughened Engineering Plastics; Collyer, A. A., Ed.; Chapman and Hall: London, 1994.
5. Flexman, E. A. Kunststoffe 1979, 69, 172.
6. Epstein, B. N.; Adams, G. C. A. In PRI Conference on Toughening of Plastics, London, 1985; Paper 10.
7. Wu, S. Polymer 1985, 26, 1855.
8. Borggreve, R. J. M.; Gaymans, R. J.; Schuijer, J.; Ingen Housz, J. F. Polymer 1987, 28, 1489.
9. Majumdar, B.; Keskkula, H.; Paul, D. R. J Polym Sci Polym Phys 1994, 32, 2127.
10. Wu, S. J Polym Sci Polym Phys 1983, 21, 699.
11. Speroni, F.; Castoldi, E.; Fabbri, P.; Casiraghi, T. J Mater Sci 1989, 24, 2165.
12. Groeninckx, G.; Dompas, D. In Structure and Properties of Multiphase Polymeric Materials; Araki, T.; Cong, Q. T.; Shibayama, M., Eds.; Marcel Dekker: New York, 1998.

13. Borggreve, R. J. M.; Gaymans, R. J.; Schuijer, J. Polymer 1989, 30, 71.
14. Oshinski, A. J.; Keskkulla, H.; Paul, D. R. Polymer 1996, 37, 4919.
15. Misra, A.; Sawhney, G.; Ananda Kumar, R. A. J Appl Polym Sci 1993, 50, 1179.
16. D'Orazio, L.; Mancarella, C.; Martuscelli, E.; Casale, A.; Filippi, A.; Speroni, F. J Mater Sci 1986, 21, 989.
17. Kunori, T.; Geil, P. H. J Macromol Sci Phys B 1980, 18, 135.
18. Gupta, A. K.; Purwar, S. N. J Appl Polym Sci 1984, 29, 3513.
19. Maiti, S. N.; Lopez, B. H. J Appl Polym Sci 1992, 44, 353.
20. Maiti, S. N.; Sharma, K. J Mater Sci 1992, 27, 4605.
21. Neilsen, L. E. J Appl Polym Sci 1966, 10, 97.
22. Nicolais, L.; Narkis, M. Polym Eng Sci 1971, 11, 194.
23. Lee, J. K.; Han, C. D. Polymer 1999, 40, 6277.
24. Lee, J. K.; Han, C. D. Polymer 2000, 41, 1799.
25. Dedecker, K.; Groeninckx, G. Macromolecules 1999, 32, 2472.
26. Bhattacharyya, A. R.; Ghosh, A. K.; Misra, A. Polymer 2001, 42, 9143.
27. Bhattacharyya, A. R. Ph.D. Thesis, IIT Delhi, 2000.